Received: 8 August 2020 | Revised: 17 March 2021 | Accepted: 17 March 2021

DOI: 10.1002/eng2.12407

RESEARCH ARTICLE

WILEY

On the design and implementation of efficient antennas for high frequency-radio frequency identification read/write devices

Ernest Ofosu Addo[1] | **Benjamin Kommey**[2] | **Andrew Selasi Agbemenu**[2] | **Hermann Kumbong**[2]

[1]Department of Information Engineering and Mathematics, University of Siena, Siena, Italy

[2]Department of Computer Engineering, Kwame Nkrumah University of Science and Technology, Kumasi, Ghana

Correspondence
Benjamin Kommey, Department of Computer Engineering, Kwame Nkrumah University of Science and Technology, Kumasi, Ghana.
Email: bkommey.coe@knust.edu.gh

Abstract

This article describes an in-depth methodical approach to the development of efficient high-frequency (HF) antennas for use in radio frequency identification (RFID) systems operating at 13.56 MHz. It presents brief theory relevant to RFID communication and sets up a framework within which features and requirements of antennas are linked to key design parameters such as antenna form-factor and size; RF power level, material and communication protocol. Tuning circuits necessary to adjust the resonance and power matching characteristics of antennas for good transponder interrogation and response recovery are discussed. To validate the approaches outlined, a stepwise design and measurement of an HF antenna for an ISO/IEC 15693 compliant read/write device (RWD) is described. Common practical problems that are often encountered in such design processes are also commented on. The prototyped antenna was tuned, connected to the RWD via a 50 Ω coaxial cable and tested.

KEYWORDS

antenna, high frequency, RFID, tuning

1 | INTRODUCTION

According to many manufacturing, energy, and service industry experts, radio frequency identification (RFID) has become arguably the most ubiquitous element for automatic identification and second only to the use of barcoded labels, in the view of others.[1,2] Although the barcode reading and other methods are still popular due to their low prices and/or longer market existence, the RFID technology has garnered a lot of interest since the turn of the millennium and its usage has been projected to see massive growth towards becoming the foremost identification method in this decade.[3] The widespread use of the RFID technology and its projected growth burst is mainly attributed to its optimal solutions to the low data storage capacity and nonreprogrammability problems associated with the other identification methods.[4] The technology's popularity is also on account of its faster, more secure and hardier means of power and data transfer between a read/write device (RWD) and a tag located on/in a remote object of interest through wireless media. Owing to

this principle of operation, RFID possesses the capability for nonline of sight and multiple object identification: two very important features required in applications like inventory control and automation.

RFID systems exist in many variants and can be differentiated by certain fundamental features. These include operation type, operating principle of data carrier, power supply, operating frequency range, and mode of data transfer. Based on the RWD transmission frequency, RFID devices may be considered low frequency (LF): 30–300 kHz, high frequency (HF): 3–30 MHz, ultra-high frequency: 0.3–3 GHz or microwave: >3 GHz systems. The HF class of RFID devices operate generally at f_{op}=13.56 MHz (wavelength, $\lambda_{op} \approx 22$ m) in the ISM band. They use inhomogenous magnetic field as means for data and power transfer; and are able to achieve read ranges up to 1 m. Like most mainstream technologies, the operation of HF devices are regulated by various standards and are also required to conform to local (national/regional) radio regulations. These include ISO/IEC 18000, 14443, 15693 standards, and the EPCglobal Class-1 HF-RFID Air Interface protocol specifications. These standards define key radio interface parameters such as modulation, subcarrier frequencies, bandwidth, and coding. Specifically, the ISO/IEC 15693 standard is designed for the so-called vicinity coupling systems: RFID devices which offer maximum read distance of up to 1 m. Tags complying with the standard are referred to as vicinity integrated circuit cards (VICCs) whiles RWDs or interrogators are called vicinity coupling devices (VCD). The three-part standard was originally designed for systems where a single or small number of VICCs are to be used at a time like access control applications. Thus, systems conforming to the standard are not so ideal for applications where large number of tag could be present in the interrogator zone. Part 1 of ISO/IEC 15693 defines the physical characteristics of VICCs.[5] In addition, this part of the standard provides some information on mechanical and EM compatibility testing.[4] Part 2 standardizes the VICC-VCD power and communications interface whiles Part 3 specifies transmission protocols and anticollision measures.

ISO/IEC 14443 is a four-part standard tailored towards proximity coupling systems: very close coupled settings where maximum interrogation range is about 10 cm thereby allowing for secure interactions. Parts 1 and 2 define mechanical properties of tags and the RF power/signal interface, respectively.[6,7] The last two parts detail anticollision measures and the transmission protocol.[8,9] Compliant RWDs and tags are termed as proximity coupling devices (PCDs) and proximity integrated circuit cards (PICCs), respectively. The standard defines two types of PICCs—Type A and B, which differ based on transmission procedures. In detail, although both types share the same transmission protocol, the two have different modulation methods, coding schemes and initialization procedures. PCDs must be able to communicate equally well by the two communication procedures, and thus support all PICC types. Typically, PCDs do this by a periodic switching between both procedures in an "idle" mode. The polling is suspended once a PICC-PCD communication link is established. Notable implementations of proximity coupling systems include biometric passports, ticketing, and some financial payment systems. The very popular near field communication technology is based in part on the ISO/IEC 14443.

The ISO/IEC 18000 standard provides a framework to define common communications protocols for internationally usable RFID frequencies. It also determines the possible multifrequency use of such protocols with minimized migration problems, implementation costs, and system management overhead.[10] Part 3 of the 18000 standard (18000-3) defines physical layer, collision management and transmission protocol parameter values for passive RFID systems with focus on item identification at 13.56 MHz. This standard is believed to have been created to address some of the aforementioned issues associated with the ISO/IEC 15693 standard. ISO/IEC 18000-3 classifies conforming systems into three noninterfering, noninteroperable modes—Modes 1, 2, and 3 which are intended to address different application areas. Mode 1 points to ISO/IEC 15693 and provides some enhancements to its item management performance. Mode 2 specifies an air interface which allows high speed RWD-tag communication links and Mode 3 combines a high-speed version of Mode 1 with optional Mode 2 features for improved performance.

Finally, the EPCglobal Network is an internet-based technology which combines data acquisition via RFID technology with documentation and location services to provide improved and precise logistics processes using unique identifiers called electronic product code (EPC).[4] The EPCglobal Class-1 HF-RFID document forms one of the basis of the EPC/RFID technology. The document specifies a signaling layer of the 13.56 MHz RWD-tag communication link, operating procedures for both end devices and a collision arbitration scheme employed in identifying a given transponder in a multitag setting.[11]

In this article, we present a methodical approach to designing efficient HF-RFID interrogator antennas which guarantees good read ranges and sensitivity to tags. Several design considerations are outlined and practical implementation options are discussed. The paper extends this discussion and applies the techniques to an ISO/IEC 15693 mid to long range system where an antenna is designed and prototyped for an industry standard RWD as a means of validation. The antenna was tuned, connected to the RWD via a 50 Ω coax line and tested.

This article is organized as follows: Section 2 reviews some theory relevant to HF-RFID communication. Next, key parameters and considerations for the design of an HF antenna are provided in a comprehensive design flow in Section 3. An experimental validation of the presented approaches are outlined in Section 4and discussed. The paper concludes with a validation in Section 5.

2 | HF-RFID RWD-TAG COMMUNICATION

HF-RFID systems, like their LF counterparts, operate based on inductive magnetic coupling, as shown in Figure 1. This sets up a two-way communication link between an RWD and a passive tag and allows for power transfer to a tag at any position inside the three-dimensional (3D) interrogation zone of the RWD. This zone constitutes the operating volume of the RWD and can be thought of as an overlap of the reactive near-fields of the two devices' antennas. A planar cut of this volume is illustrated by the faint blue shape in Figure 1. Here, the RWD antenna coil transmits a query by generating a strong amplitude modulated magnetic field. The time-varying field flux crosses the cross-section of the nearby tag antenna coil thereby inducing a voltage at the tag's antenna ports. This voltage is stepped up in a resonant circuitry, rectified and serves as power supply for the tag chip. As shown in Figure 1, the resonant circuit is formed from the capacitor C_1 and the tag antenna impedance Z_t whiles the rectifier circuit is an envelope detector consisting of the capacitor C_2, diode, and the tag chip input impedance, Z_{chip}. The draw on magnetic energy by the resonant tag creates feedback on the RWD antenna which is often represented as a complex transformed impedance, Z_F at the RWD antenna coil given by Equation (1). Provided the mean dimensions of the antennas are small compared with λ_{op}, the RWD-tag system could be represented by the equivalent lumped element model in Figure 2.

$$Z_F = \frac{(\omega_{\text{op}}\gamma(d))^2 L_t L_d}{Z_t + Z_{\text{chip}}}, \quad \gamma(d) \in [0,1], \tag{1}$$

where $\omega_{\text{op}} = 2\pi f_{\text{op}}$ whiles $\gamma(d)$ is the coupling coefficient. $\gamma(d)$ depends on the distance between the two antennas, d and their (equivalent) radii, r_t and r_d as stated in Equation (2) assuming that the two antenna coils are positioned parallel to each other and aligned on a common central axis; and provided $r_d \geq r_t$. If coils deviate from this parallel position, the orientation of the tag loop in space is resolved with respect to the RWD antenna by appropriately weighting $\gamma(d)$.

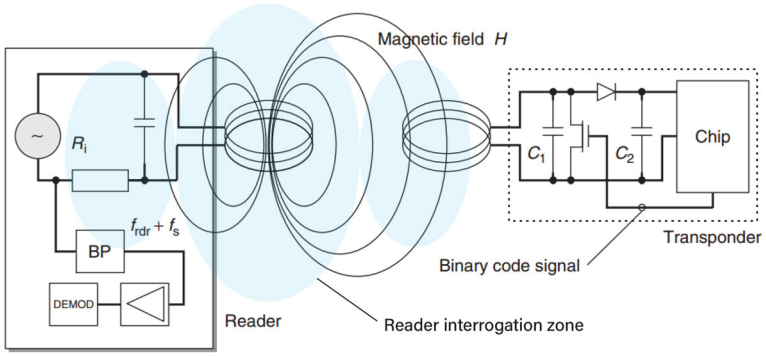

FIGURE 1 Operation of an HF-RFID system. HF, high frequency; RFID, radio frequency identification

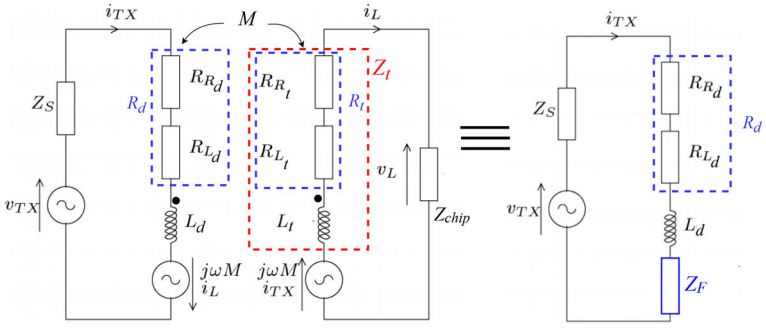

FIGURE 2 Near-field equivalent lumped element model showing the introduction of Z_F at the RWD. R_d and R_t are the self-resistances of the RWD and tag antenna coils, respectively. The RWD is represented by a voltage source v_{TX} with a series impedance Z_S. RWD, read/write device

Furthermore, it could be shown that $\gamma(d)$ is qualitatively related to the self-inductances of the antennas, L_t and L_d; and their mutual inductance, M (Equation (2)).[4,12]

$$\gamma(d) \approx \left(\frac{r_t r_d}{d^2 + r_d^2}\right)^{\frac{3}{2}} = \frac{M}{\sqrt{L_t L_d}}. \tag{2}$$

In the tag, by switching a load (ohmic or capacitive) using data pulses in the tag's circuitry, Z_F varies and voltage at the RWD antenna output changes accordingly. This is called load modulation and it is used as a means by the remote tag to signal its unique identification or any other data to the RWD as an answer to its query. In practical systems, this signaling isn't strong enough and hence not very distinguishable from the RWD's significantly stronger signal. A more robust technique known as load modulation with a subcarrier is often employed where the switching of additional load creates a new high elementary carrier at frequency, f_{sub} called a subcarrier. In 13.56 MHz systems, typical f_{sub} values include $f_{\text{op}} \times 2^{-n}$ where $n = 4$, 5, and 6. As shown in Figure 3, the subcarrier is first amplitude modulated in time with the data to be transmitted, creating two spectral lines at $\pm f_{\text{sub}}$. The modulated subcarrier is then used to modulate the carrier f_{op}. This shifts the two sidebands to frequencies $f_{\text{op}} \pm f_{\text{sub}}$. The data flow rides on these modulated sidebands which upon transfer, could be easily extracted, conditioned and demodulated at the RWD receiver front-end.

In vicinity coupling systems, the RWD-to-tag or forward path communication uses 10% or 100% amplitude shift keying (ASK) with pulse position modulation (PPM) coding. Two PPM schemes are common with vicinity systems: 1-of-4 which gives the "fast mode" and 1-of-256 for the "long-distance mode." With 1-of-4 PPM, queries can be sent a rate of 26.48 kbit/s whiles a 1.65 kbit/s rate is achieved with 1-of-256 PPM. For tag reply on the return path, the tag reply is sent either as a 100% ASK pulse-shaped signal on a 423.75 kHz subcarrier or a frequency shift-keyed signal switching between 423.75 and 484.12 kHz subcarriers. In both cases, replies are encoded with Manchester code and data rates of about 6.6 or 26.6 kbit/s can be achieved.[13] The two forward path modes coupled with the possibility to use one or two subcarriers in the

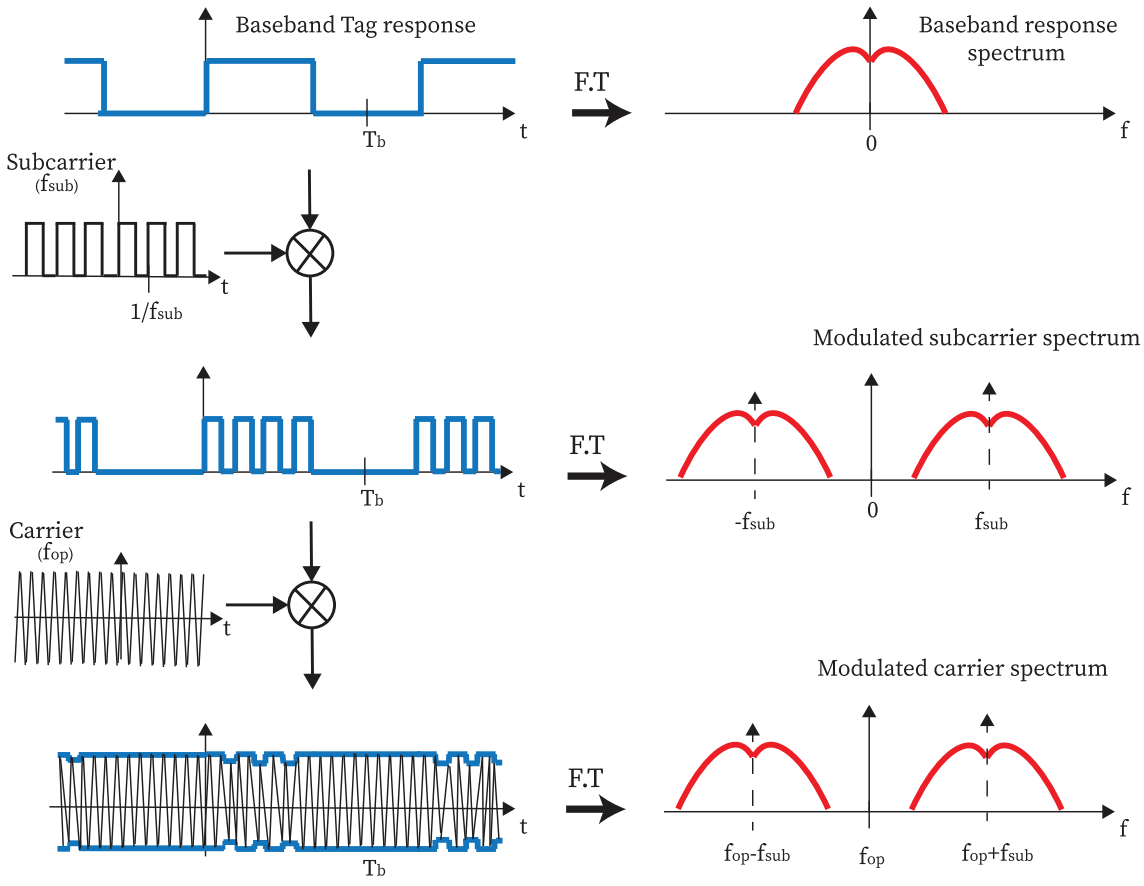

FIGURE 3 Load modulation of the baseband tag response with a subcarrier

tag replies makes the ISO/IEC 15693 interface quite flexible. This allows vicinity systems to be tuned to suit different operational requirements ranging from use with low RF noise at long range to high RF noise at short range.

For ISO/IEC 14443 conforming systems with Type A cards, a 100% ASK modulation with modified Miller bit encoding is used in the forward transfer. For the return link, an on/off keyed 847 kHz subcarrier is modulated with a Manchester coded reply. In Type B, PCD-to-PICC data transfer is achieved with a 10% ASK modulation with nonreturn-to-zero (NRZ) coding. In its response, the PICC uses an 847 kHz subcarrier which is binary phase shift keying (BPSK) modulated with a NRZ coded reply. For both Type A and B, the baud rate in both forward and return transfer directions is 106 kbits/s.[4,7]

ISO/IEC 18000 Mode 1 uses the "Interrogator-talks-first" (ITF) technique similar to ISO/IEC 15693 and achieves speeds of about 26 kbit/s. In Mode 2, a $\pm 3°$ to $\pm 4°$ phase jitter modulation (PJM) of the powering field coupled with modified frequency modulation (MFM) encoding is used for RWD to tag transmission. The total forward link data rate for Mode 2 is fixed at 424 kbit/s. Here, RWDs can be full duplex providing the possibility for transmitting queries whilst receiving multiple tag replies simultaneously. On the other hand, the return path employs an MFM-encoded, BPSK modulated subcarrier and eight simultaneous reply channels allowing for a maximum achievable path speed to 848 kbit/s (each channel is 106 kbit/s). Tags can select from one of the eight subcarrier frequencies which range between 0.969 and 3.013 MHz. Tag replies are band limited to reduce data and subcarrier harmonic levels, enabling the simultaneous reception of information from tags transmitting on the different channels. Tags are half duplex. With Mode 3, compliant systems use ITF with random slotted anticollision medium access. The air interface uses a mandatory ASK modulated pulse-interval encoded (PIE) communication and gives a higher speed air interface (higher than ISO/IEC 15693). Mode 3 RWDs are also able to recognize large quantities of tags in the field. Data rates include a 100 kbit/s forward link speed and 424 kbit/s or a maximum of 848 kbit/s on the return path. Slower rates are also available. There is also an optional PJM modulated, MFM-encoded communication with PJM compliant tags. Available speeds for this method are 212 kbit/s forward link and a 106 kbit/s/channel for tag-to-RWD transmissions.[10]

In the EPCglobal Class-1 case, reader-to-tag communication employs PIE encoding with ASK (double-sideband, single-sideband or phase-reversal) and can achieve a maximum data rate of about 160 kbits/s. In response to the RWD query, the tag uses ASK or PSK with FM0 baseband for single-reader mode or Miller modulation with a 40–640 kHz subcarrier for multi/dense-reader mode. The dense-reader mode is useful for preventing adjacent readers from interfering. Transmission rates range from 5 to 640 kbit/s.[11]

3 | ANTENNA DESIGN

3.1 | Design considerations

Based on their operational principle, HF-RFID antennas are typically designed as electrically small loops. Designing RWD antennas for optimum performance requires knowledge of the complete RFID system's specifications such as RWD front-end, antenna RF feed and possible tag characteristics. Since most systems operate at 13.56 MHz, antennas are to be tuned to that frequency and have an impedance that matches the RWD feed with a minimal reflection loss. Furthermore, when connected to the antenna, the RWD must exhibit a very good frequency selectivity in order to capture tag responses. Another important design goal is the maximum read distance of tags, $d_{\max}$. Since passive tag hardware depends on field launched by the RWD for power, the RWD antenna must be designed such that the magnetic field it produces at $d_{\max}$ is sufficient for both tag chip operation and RF communication. The transformer-type magnetic nature of the RWD-tag coupling implies that $d_{\max}$ cannot be very large and that the read distance must be confined to the reactive near field of the antenna, that is, $d_{\max} << \frac{\lambda_{op}}{2\pi}$. Indeed, the interrogation magnetic field **H** can be shown to attenuate rapidly beyond a certain distance with a decay of about 60 dB per decade in free space.[4] Moreover, if the tag is located outside the near field region, it will receive a traveling wave instead of a quasi-static **H** field and the modifications to the field due to the presence of the tag will never be sensed by the RWD. Such a quasi-static **H** field is guaranteed in the near field if the coil is supplied with a constant current.

3.1.1 | Form factor and sizing

Loop antennas are inexpensive, versatile and can take the form of numerous easily constructible shapes. They are particularly suited HF-RFID systems which depends solely on near-field magnetic induction for power transfer and

wireless communication. For short-range inductive radio links, the circular loop is often preferred. This is because the current on the entire antenna is in phase and as such contribute constructively to the **H** field at a given distance d from the loop. Under the constant loop current assumption, the **H** field produced is found to achieve its largest strength at a certain ratio of the loop radius, r_d to d ($\xi = \frac{r_d}{d}$). That is, for every $d_{\max}$ specification, there exists an optimal r_d. Taking into account the phase difference along the total loop length, a compact cylindrical/circular antenna coil of radius r_d (i.e., total thickness, $t << r_d$) produces a magnetic field with component at an observation point P along the center line perpendicular to the coil's plane, $\mathbf{H}_x$ with magnitude given by Equation (3) (refer to Figure 4).

$$|\mathbf{H}_x| = \left| \int_0^D \frac{I \cos\theta e^{2\pi f_{\text{op}} l}}{4\pi(d^2 + r_d^2)} dl \right| = \frac{I r_d \sin(\frac{2\pi^2 d}{\lambda_{\text{op}}})}{4\pi^2 \sqrt{(d^2 + r_d^2)^3}} \left| \sum_{n=0}^{N-1} e^{j\frac{4\pi^2 n r_d}{\lambda_{\text{op}}}} \right|, \tag{3}$$

where $D = 2\pi r_d N$ is the total length of the loop material, N is the number of loop turns, I is the loop current amplitude and θ is the loop's tilt angle indicated in Figure 4.

The optimal ξ value can be found by computing the limiting case, $d \to 0$, of the null-derivative condition for $|\mathbf{H}_x|$, that is, $\frac{\partial |\mathbf{H}_x|}{\partial \xi} = 0$. An elaborate derivation of the general N case of this condition is performed in Reference 14. A simplified approach for the case of a single turn loop is shown in Equation (4).

$$\lim_{d \to 0} \frac{\lambda_{\text{op}}(2\xi^2 - 1)}{\xi} - \frac{2\pi^2 d(1 + \xi^2) \sin\left(\frac{4\pi^2 r_d}{\lambda_{\text{op}}}\right)}{1 - \cos\left(\frac{4\pi^2 r_d}{\lambda_{\text{op}}}\right)} = 0. \tag{4}$$

The solution to Equation (4) shows that, for optimal performance, $r_d = \sqrt{2}d$.[15,16] The result also holds for any given N. It should be noted that although a loop with radius $r_{d(\text{opt})}$ is required for optimal performance of tags, an accurate assessment of a system's $d_{\max}$ requires knowledge of the minimum interrogation field strength, $H_{\min}$ of the tag to be used. That is the tag can still be sensed until a distance corresponding to the larger of the two intersection points of the $|\mathbf{H}_x|$ vs r_d curve and the line $|\mathbf{H}_x| = H_{\min}$ for a given current and number of turns. The derived condition suggests that longer read distances can be achieved by increasing the loop radius accordingly. However, this relationship is limited by the constant current precondition. The alternating current fed from the RWD front-end can be assumed to be constant if D is small compared with λ_{op}. As a rule of thumb, the condition $D < 0.2\lambda_{\text{op}}$ is often used. Under this assumption, the static field strength at point d from Equation (3) can be simplified as shown in Equation (5) using the Biot–Savart law.[17]

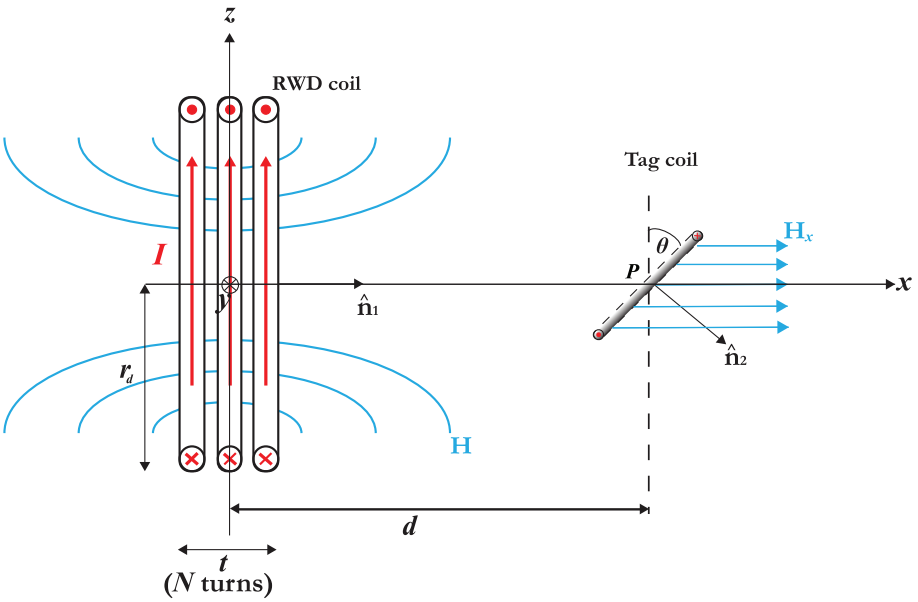

FIGURE 4 Loop antenna geometry and path of magnetic flux lines

$$|\mathbf{H}_x| = \left| \frac{NIr_d^2}{2\sqrt{(d^2 + r_d^2)^3}} \right|. \tag{5}$$

When considering small loops with optimal radius, Equation (5) gives a notion that for a given current source, by taking more turns, the loop will produce a large **H** field at the tag position *P*. However, this is not necessarily true and the use of more loop turns becomes counter-productive even for moderately high *N*. With high *N*, the total loop length *D* becomes considerable with respect to λ_{op}. In such a case, there exists more current carrying conductor parts which contribute to the **H** field. These contributions are weaker due to the increased distance from these current carrying parts to point *P* hence the total field at the tag is very weak. In addition, due to the phase differences along the larger loop, the contributions of all loop parts will be out of phase at *P* resulting in partial destructive interference, exacerbating the dip in field strength.[14] Furthermore, for *D* equal to $0.5\lambda_{\text{op}}$, or a multiple, standing wave effects are noticed. The loop experiences self-resonance, affecting the usability of the loop in the antenna set-up as the design of required current enhancing techniques (discussed in Section 3.2) is difficult and highly constrained. In cases like this, the antenna system will resonate at multiple frequencies and the energy will be divided amongst them.[14,18] It is noteworthy that if such enhancement techniques are employed, read distances *d* can be achieved with smaller radii r_d, that is, $r_d < \sqrt{2}d$ since the feed current is amplified. The value of r_d would depend on the nature of the enhancement circuit but a conservative choice in such a case is $r_d \approx 0.5d$.

Power transferred in the antenna near-field region is predominantly inductive. Hence, the antenna's reactive impedance is of primary importance although its real part cannot be neglected. Provided the $D < \lambda_{\text{op}}$ condition is met, a loop antenna can be modeled fairly accurately with lumped components as shown in Figure 5. The real component of the loop conductor's internal impedance is due to ohmic phenomena like skin and proximity effects. *L* is the loop inductance whiles the parasitic per unit length capacitance between each pair of turns is quantified by C_p. For a loop made of solid wire with radius *b*, the ohmic resistance could be evaluated using Equation (6). The reactive quantities, *L* and C_p of such a loop are given in Equations (7) and (8).[15,19] σ, μ, and ϵ are respective notations for the wire conductivity, magnetic permeability of medium and the electric permittivity of the wire insulation. In the absence of insulation, $\epsilon \to \epsilon_o = 8.85 \times 10^{-12}$ F/m. It should be noted that equations for evaluating the lumped quantities may vary slightly depending on the shape of loop and the nature of materials used. As examples, expressions for square/rectangular loops are discussed in Reference 15 and that for loops formed from hollow conductor tubes are given in Reference 20.

$$R = \frac{Nr_d}{b} R_s \left(\frac{R_p}{R_o} + 1 \right) \tag{6}$$

$$L = N^2 \mu r_d \left(\ln \left[\frac{8r_d}{b} \right] - 2 \right) \tag{7}$$

$$C_p = \frac{2\pi^2 r_d \epsilon}{\ln \left[\frac{t}{2bN} + \sqrt{\left(\frac{t}{2bN} \right)^2 - 1} \right]}, \tag{8}$$

where $R_s = \sqrt{\frac{\omega_{\text{op}}\mu}{2\sigma}}$ is the surface impedance of the loop conductor, R_p denotes the per unit length proximity effect ohmic resistance, and $R_o = \frac{\text{NR}_s}{2\pi b}$ is the per unit length skin effect ohmic resistance. The ratio $\frac{R_p}{R_o}$ is discussed in Reference 15 as a

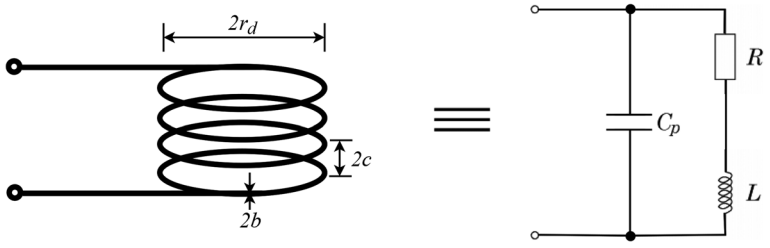

FIGURE 5 Equivalent lumped parameter circuit model of multiturn loop antenna

function of the ratio $\frac{c}{b}$ for loops with $2 \leq N \leq 8$ with an interturn spacing of $2c$. In that analysis, it is shown that for close spacing ($\frac{c}{b} \to 1$), R is twice as large as that in the absence of proximity effect, that is, $\frac{R_p}{R_o} = 0$. From Equations (6) and (7), it is easy to infer that loop's resistance R is very small compared with the inductive impedance $\omega_{\text{op}}L$. To study the relation between loop's inductance and the strength of the **H** field it generates, the antenna is considered to be fed by a voltage source V_d in the RWD front-end. From Equation (5), the **H** field generated is directly related to the magnetomotive force, MMF in the RWD equivalent magnetic circuit. Discarding the small R and high impedance shunt loading of V_d by C_h; and employing Ampere's circuital law:

$$\text{MMF} = NI = N\frac{V_d}{\omega_{\text{op}}L} = N\frac{V_d}{\omega_{\text{op}}} \times \frac{S}{N^2} \propto \frac{V_d S}{N}, \tag{9}$$

where S is the reluctance of the magnetic circuit and essentially represents the inverse of the inductance L' of single turn loop with the same cross-sectional area. Therefore, affirming aforementioned sizing criteria to maximize $|\mathbf{H}_x|$, it is best to use an optimally small size single turn loops made of large diameter wire, that is, $N = 1$ and small L'. Furthermore, by using the single turn loop, the problem of high ohmic losses due to proximity effect is eliminated. This is especially good for the communication properties of the RFID system. This is because the larger loop resistance translates to higher antenna thermal noise whose voltage spectral density is described by the Johnson–Nyquist formula ($\overline{v_n} = \sqrt{4kTR}$). Therefore, in the receive mode, though the signal level at the antenna output may be large, the signal-to-noise ratio (SNR) is poor and faint tag responses may be lost in the background noise. In addition, with large (multiloop) antennas, it is often difficult to meet legal transmitted power guidelines from local and international regulatory bodies such as the ETSI and FCC in Europe and the USA, respectively. According to the ETSI EN 300 330 standard, the strength of the generated magnetic field measured at 10 m should be at most 42 dBμA/m.[21] Usually, larger loops are barely able to comply with this regulation and require extra special shielding to operate within this limit.[22] Other issues with large loops include the emergence of magnetic flux holes in the interrogation zone resulting in insensitivity to some tags and the very high loop L (Equation (7)) which may make power matching very difficult to achieve. However, in cases such as longer range systems where larger loops must be used, field shaping techniques such as the use of so-called magnetic field repeaters could be employed.[23] Alternatively, in order to eliminate or correct flux dead zones, an array of smaller independent and appropriately distributed loops could be used rather than a single large coil.[24]

3.1.2 | Construction methods: Materials and technologies

Each HF-RFID application is unique and techniques used in realizing the RWD antennas may vary from one use case to another. Loops can be made from any conductive material provided the structure is constructible. Such materials may be general purpose or rather closely associated with a particular construction technology employed. Commonly used conductors include copper (Cu) and aluminum (Al). Some Cu alloys like brass are also sometimes used, albeit not very common. Cu has been and largely remains the material of choice due to its superior conductivity and relative strength. Al has been touted and explored as an attractive substitute to copper due to its comparable electrical properties and additional advantages of abundant availability, lightness and lower cost. However, aluminum poses challenges in construction processes like soldering and may require some special care, tools, or materials. For instance, since most commercial cables and connector elements are Cu-based (Cu/brass core or Cu-clad steel), the use of aluminum for loops make the coils highly susceptible to corrosion due to the high electrochemical potential buildup at Cu-Al contact areas especially when antennas are used in humid outdoor spaces. With time and use, the continuous galvanic action severely degrades the antenna's electrical and structural performance. In addition, such dissimilar metal contacts could result in high resistance connections which can alter the antenna response. Counteracting the aforementioned effects require treatment such as tin-plating copper contacts to slow the galvanic attack. Alternatively, same material cables and contacts could be used.

Another popular material for antenna realization is silver (Ag), which is the most electrically conductive metal available, only ~7% better than Cu in this regard. However, Ag is less dense compared with Cu, thus on a resistivity-to-mass basis, the two materials are quite identical, with Ag being the rarer and more expensive of the two. Cu is more ductile and malleable than Ag and can be shaped easier and stressed without damage. On the other hand, wires drawn from Ag are susceptible to crack when twisted or kinked. Consequently, Ag is reserved for printing antennas in the form of inks and pastes; a procedure which will also need curing for maintaining structural integrity of coil tracks. However, Ag inks are

quite resistant to oxidation, which is a major weakness of both Cu and Al inks. When printed, Cu traces must be coated with masks to prevent corrosion. Recent innovations such as the Cu nanoparticle technology has produced Cu inks which are easily printable, hardy to oxidation, and have great electrical performances.

Available methods of constructing HF loop antennas range from the use of conductive tubes to screen printing. Tube antennas are very robust and can be created from standard pipes and fittings. However, they are often bulky and can be tough to work with, especially for circular loops. Hence, such antennas are molded as simple polygons in order to easily achieve neater loops. Tube antennas require large driving sources and oft complex unstable structures for tuning and current enhancement. In addition, for good ohmic contacts, construction of antennas with tubes require special tools and skills such as high power blow-torch soldering/brazing. Nonetheless, compared with other technologies, tube antennas are known to provide large read ranges provided they are driven high enough.[25] In cases where higher RF output power may be required, an external power amplifier locked at f_{op} could be introduced at the RWD output. HF-RFID interrogator antennas could also be made from conductive-backed tapes.[22] Unlike the tube ones, tape antennas are very simple and less bulky. However, they are not hardy and require some protection from environmental conditions.

For miniature systems, antennas can be created on PCBs and interfaced directly and neatly with onboard single-chip transceivers such as the NXP CLRC632 and TI TRF79xxA series. With fully onboard modules, the sizes of antennas must be controlled as a very large antenna may not be properly driven by the low output power RWD chip (~200 mW at 5 V). Thickness of substrate and distance between trace windings are key additional factors affecting the performance of PCB antennas. Very thin substrates could cause fluctuations in μ values and loose loop windings could decrease L.[26] However, it should be noted that the tightness of windings is limited by the manufacturing process. Such antennas may be etched by an average skilled person and do not necessarily require industry-grade processes or equipment. However, etching PCB antennas involve the use of harmful materials such as ferric chloride acid, hence the manufacturing process should be carried out meticulously and with safety equipment.

A relatively new printing technique for realizing HF loop antennas is screen printing conductive patterns with pastes or inks onto low cost flexible substrates such as paper, polyethylene terephthalate (PET), polyimide, or polylactic acid (PLA).[27] Ag particle and nano Cu inks are common printing materials for antennas where a coil resolution of 50 lines/cm and a track thickness as low as 11 μm is achievable.[28,29] For substrates, paper is the popular choice for these antennas due to its biodegradability and ultra-low cost. Moreover, it is resistant to thermal deformation, which is beneficial to the curing of printed conductive tracks. However, paper substrates require special coating before use for antenna printing, has limited mounting methods for surface mounted device (SMD) components, and its relative permittivity is not very stable with environmental changes, for example, moisture and temperature. Depending on the SMD package, the component could be mounted on cured ink tracks by using either hot air soldering with low temperature paste (like Sn42/Bi57.6/Ag0.4), fixing with Ag epoxy glue or applying both methods together.[24] PET is another low cost substrate option. PET is not widely used since it is not environmentally friendly and deforms when heated; in addition to its limited SMD mounting techniques. Polyimide solves the problem of temperature endurance and supports conventional SMD mounting technology (SMT) like reflow soldering. Nonetheless, the use of polyimide is unattractive because it is expensive to use and a possible environmental pollutant. Like paper, PLA is biodegradable and nontoxic. Furthermore, PLA substrates are themselves 3D printable and are available in both rigid and flexible forms. High fabrication complexity, low temperature endurance, and limited SMT are some drawbacks of PLA use.[30] In HF-RFID technology, screen printing has mostly been used for manufacturing flexible transponders for applications like electronic article surveillance[31] and environmental monitoring.[32] For RWDs, this printing technique is particularly useful in configuring antennas for handheld systems, large areas, and nonflat surfaces. Despite the low cost and great design flexibility advantages of this method, printed antennas are plagued with reduced read performance (poor frequency selectivity and low SNR).[33,34] These problems can be alleviated by using special curing techniques to condense the microstructures of the printed antenna coils.[24] In addition, applying the conductive inks multiple times on the same coil track has been reported to reduce the DC resistance to tolerable levels.[35] However, the thick film technique increases the overall cost and difficulty of the screen printing process.

Wire antennas are typically preferred as they provide a good balance of the pros and cons discussed above. These are the simplest of all the available methods and wire used could be bare or insulated.

3.1.3 | Environmental influences

The setting in which the antenna would be used, as well as its final mechanical casing, if any, are key to antenna performance and hence should be considered carefully. The presence of any metal (including other antennas) in close proximity

to the loop, dampens and decreases the loop L hence detuning the antenna. In addition, eddy currents in the metal generates an opposing **H** field and lower sensitivity to tag response signals.[36] These phenomena degrade the antenna's read range performance and the minimum separation from metal for noticeable detuning effects, grows with the loop size. For unavoidable exposure to metal, ferrite backing could be employed. This is a technique where a ferrite sheet is introduced to screen the loop from metal thus limiting detuning effects and improving antenna performance. Generally, it is advised that antennas always be tuned in their final positions or enclosures to account for inductance changes caused by both the metal and ferrite sheet.[26]

Radio noise is another classical influence on antenna performance. Depending on the levels, radio noise can severely reduce RWD receiver performance and limits its read range. Thus, noise sources are to be identified by surveying the site, preferably before starting the antenna design. Indoor electronic appliances, industrial equipment, and broadcasting radios are common sources due to the unwanted radio emissions from their electrical oscillators employed. Locating such interference at HF could be done using the approach explained in Reference 37. The antenna must also be sufficiently shielded to lessen the effect of such noise.

Interaction of physical elements of the environment with loop material also affect antenna performance. As discussed in Section 3.1.2, Cu and Al antennas corrode in humid and warm space. This phenomenon is worse in areas near salty water bodies. In such environment, Al oxidizes readily and a hard outer layer of electrically insulating oxide quickly forms around and strongly attaches to the metal. For Cu, components oxidize upon exposure but the oxide formed is relatively soft and conductive, although not as conductive as the base metal. These changes in the conductor alter antenna parameters like the voltage standing wave ratio. When bare Al or Cu is used, conductors must regularly be wire brushed to remove the oxide layer. A more effective solution is to use tin-coated cable and connectors whiles applying oxide inhibiting compound immediately during installation. In PCB antennas, resins like epoxy are used to mask conductive traces for this purpose. For tape antennas, the conductive material tends to peel when exposed to ultraviolet light, humid climates and fluctuating temperatures. In very cold temperatures, tapes lose tack and adhesion. They crack and become brittle. Conversely, when the environment is too warm, tapes may become soft and adhesives begin to break down and run. Extra adhesive suited for the corresponding surrounding conditions should be used to reinforce tapes. For example, rubber adhesives are good for temperatures in the range −5–60°C whiles silicone or acrylic adhesives are effective for extreme temperatures. Generally, efforts must be made to regulate the environment or shield antenna assembly from the elements by using appropriate enclosures.

3.2 | Tuning and current enhancement network

Standards for HF-RFID systems specify the minimum interrogation magnetic field strength, $H_{\min}$ to be produced by RWD antennas for proper operation of tags, that is, to build up a high enough voltage to power up the tag hardware. The ISO/IEC 15693 specifies $H_{\min} = 0.115$ A/m (rms) whiles the ISO/IEC 14443 standard recommends $H_{\min} = 1.5$ A/m (rms).[7,13] However, it should be noted that there are tags from some manufacturers that are designed to operate very well with less (e.g., for NXP cards, $H_{\min} = 0.09$ A/m). Let us study a VCD antenna design case where the desired maximum read distance is 0.6 m. Using the optimal radius criterion with Equation (5) yields Equation (10). With $R < \omega_{\text{op}} L$, the voltage to be applied to the RWD antenna to achieve d is given in Equation (11) where $I_{\min}$ is the minimum rms current needed in the antenna for $H_{\min}$. For a single turn loop with $L = 1.5$ μH, $|V_d| \approx 60$ V. Feeding the loop with such high voltage directly from the RWD front-end is not practical, hence enhancement techniques are required. This can be done either actively with the aid of an amplifier (e.g., Class E) or passively by means of an RLC circuit.

$$|\mathbf{H}_x| = \left| \frac{NIr_d^2}{2\sqrt{(d^2 + r_d^2)^3}} \right| = \left| \frac{\text{NI}}{\sqrt{27}d} \right| \tag{10}$$

$$|V_d| \approx I_{\min} \times \omega_{\text{op}} L = \left| \frac{\sqrt{27}\omega_{\text{op}} d H_{\min} L}{N} \right|. \tag{11}$$

The extent of enhancement is not unbounded. In a passive approach, this can be quantified by the quality factor Q of the resonator. In the tag-to-RWD communication, the modulated tag response is captured by the RWD antenna and

relayed to the receiver front-end for demodulation. The received signal is conditioned and the subcarrier signal in the spectrum sidebands are extracted. Although guaranteeing larger RF power for the loop antenna, a large $Q = \frac{f_{op}}{BW}$ results in narrower bandwidth BW which conflicts with the RWD bandpass characteristics resulting in poor carrier-subcarrier separation. Furthermore, the RWD becomes susceptible to ringing issues which could interfere with protocol parameters such as bit timing.[29] A good compromise is to design for sufficient bandwidth allowing the undistorted reception of a modulated carrier signal whiles having enough power to meet the H_{min} criterion. For ISO/IEC 14443 applications, the standard prescribes Q ranging between 6 and 10 and for ISO/IEC 15693 systems, the loaded antenna's Q must lie in the range of 15–20 for good performance (Figure 6).[5,6] The more relaxed Q requirement for vicinity coupling systems is because they have lower f_{sub} and lower data rates as compared with PCDs, hence requiring narrower bandwidths (see Section 2). To design applications that comply to both standards, $Q = 7$ is recommended.[26]

To enhance the current, the antenna must be made to behave as a parallel RLC circuit or slight variant of it. From Equation (8), it can be assumed that the impedance due to C_p is high enough at f_{op} and that the antenna loop is equivalently a series RL circuit as shown in Figure 8. Hence, the antenna is approximately a single time constant system whose dynamics are described by a large time constant $\tau = \frac{L}{R}$. Therefore, the unloaded quality factor of the antenna, $Q_o = \omega_{op}\tau$. The large Q_o could be reduced to an overall recommended value, Q_L by loading the antenna with a large shunt resistance R_{par} to produce an effective antiresonance with a lower quality factor $Q_{ext} = \frac{R_{par}}{\omega_{op}L}$. Since $R_{par} >> R$, it can be proven that $Q_L = Q_o||Q_{ext} \approx Q_{ext}$. Therefore, in designing damping network, a desired Q_L is first selected and the appropriate shunt resistor value can be determined as $R_{par} \approx \omega_{op}LQ_L$. This resistance value could be fine-tuned for optimum performance. To achieve a parallel RLC chain which resonates at f_{op}, a (tunable) capacitance $C_{par} = \frac{1}{\omega_{op}^2 L}$ should be introduced into the network.

Finally, when isolated from the tag, the impedance of the loop antenna together with the enhancement and tuning networks should be matched to the RWD source impedance, Z_s. Matching ensures that maximum power leaves the RWD and also prevents undesired effects such as parasitic power emissions and power reflections which may arise due to the nonstationary nature of RF voltages at HF frequencies. In typical industrial RWDs, $Z_s = 50\ \Omega$ and hence 50 Ω coaxial (or shielded) cables are used to feed antennas. To achieve power matching between the antenna and the RWD output module via the coax supply, the damped antenna impedance $Z_{in} = (R + j\omega_{op}L)||R_{par}$ must be transformed to $R_X = 50\ \Omega$. There are numerous techniques for matching antennas, some suitable for some construction technologies than others. Common methods include T-matching, gamma matching, and transformer matching. A technique which combines tuning, enhancement, and matching in a compact way is capacitance matching with damping. This technique is essentially an all-capacitor L-section since Z_{in} falls outside both unit resistance and conductance circles on the Smith Chart. Here, C_{par} is split into series and shunt elements C_s and C_h adding an extra degree of freedom to the network design. C_s shifts Z_{in} in the direction of the jX axis shown in Figure 7 (i.e., unto the unit conductance circle), while C_h shifts the impedance point away from the origin in a circular path in the z plane (i.e., along the unit conductance circle to R_X). A simplified dimensioning of the shunt and series capacitance elements from C_{par}, R_X, and R_{par} are approximated in Equations (12) and (13), respectively. The values obtained for C_h and C_s are not exact and may need tuning. The circuit is then adapted to function as a balun to eliminate common mode noise, ringing and other effects due to the large voltage difference between the coax core and the outer grounded shield. Figure 8 shows the balanced version of the capacitance matching circuit.

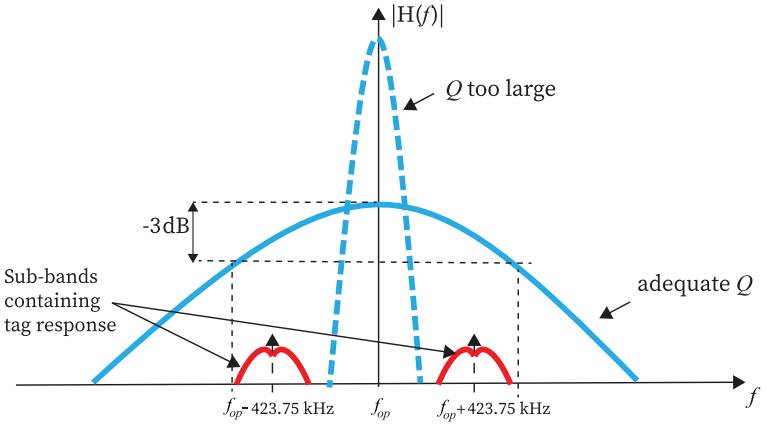

FIGURE 6 Bandpass characteristics observed for read/write devices with adequate and very high Q antennas

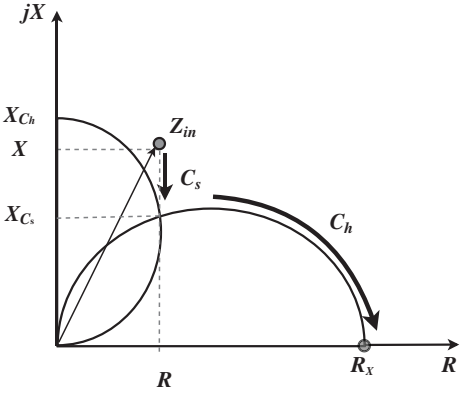

FIGURE 7 Z plane representation of Z_{in} transformation by C_s on C_h

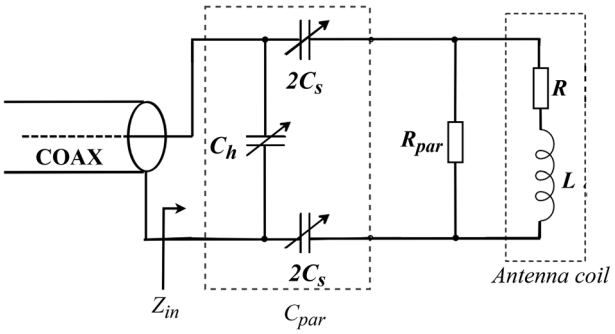

FIGURE 8 Circuit representation of damped loop antenna with a capacitance matching network

$$C_h \approx C_{\text{par}}\sqrt{\frac{R_{\text{par}}}{R_X}} \tag{12}$$

$$C_s = \frac{C_h C_{\text{par}}}{C_h - C_{\text{par}}}. \tag{13}$$

4 | EXPERIMENT

A single turn circular loop HF antenna was designed, prototyped, and tested for read range $d_{\max} = 0.6$ m to validate the discussed methods and formulas. Following considerations in Section 3.1.1, the antenna was formed from 1 mm diameter copper wire and molded into a loop of radius $r_d = 0.3$ m on a cardboard substrate. From Equations (6) and (7), the impedance of the antenna at f_{op} was estimated to be $0.59 + j208.02\ \Omega$. The antenna was modeled in CST Microwave studio and its impedance was simulated to confirm the results obtained from the analysis. The simulated input impedance was $0.64 + j215.69\ \Omega$. The model of the antenna loop and its impedance plot is shown in Figure 9. Figure 10 shows the simulated magnetic field strength produced in the plane perpendicular to the loop plane. The input impedance of the realized antenna was determined by first measuring the complex power reflection coefficient Γ at the antenna port using the Agilent E5071c vector network analyzer and a balun (Figure 11(B)). The measured input impedance of the antenna at f_{op} was then obtained from Γ as $Z_{\text{in}} = 2.25 + j211.48\ \Omega$ using Equation (14). The simulated and measured loop reactances bore close agreement. However, there was a discrepancy between the calculated and measured resistances which may be attributed to error in loop sizing, difference in material properties (simulated and prototyping), or other sources of ohmic losses such as imperfect circuit contacts.

$$Z_{\text{in}} = \frac{50(1-\Gamma)}{1+\Gamma}. \tag{14}$$

The unloaded Q of the antenna coil was $Q_o \approx 94$, which was about five times the recommended limit. Designing for Q_L=18, a shunt resistor $R_{\text{par}} = \omega_{\text{op}} L Q_L \approx 3.80\ \text{k}\Omega$ was used as an initial design value. Capacitance matching was used to

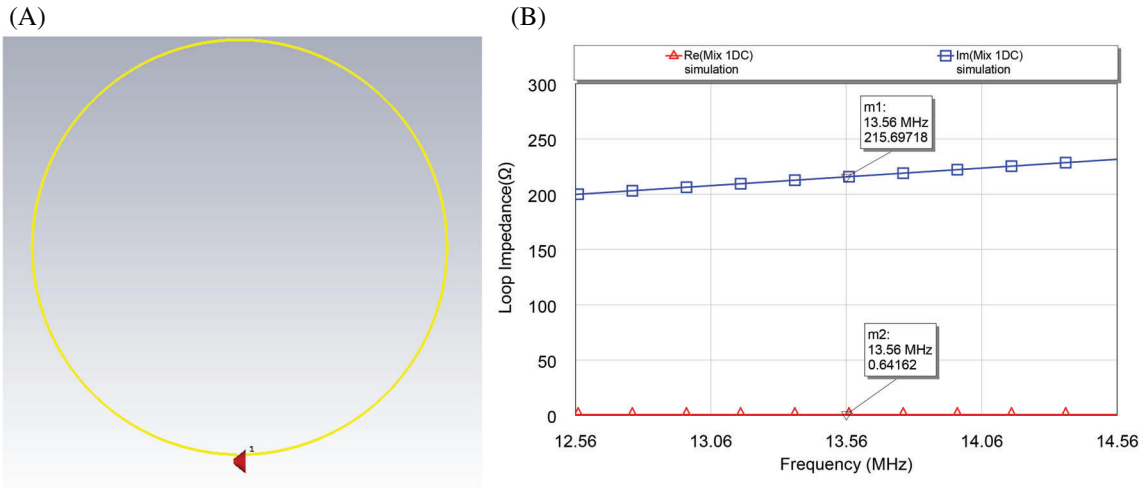

FIGURE 9 Model and simulation of input impedance of the loop antenna

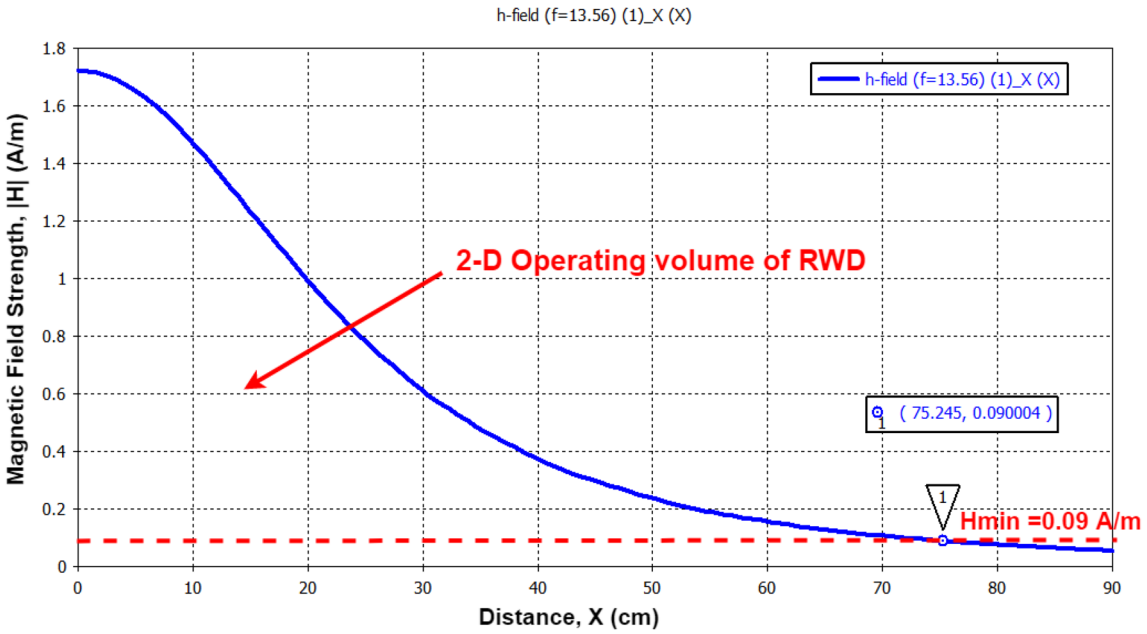

FIGURE 10 Plot of simulated $|\mathbf{H}_x|$ as a function of distance in cm. Area under the curve bounded by the reference tag $H_{\min}$ represents the two-dimensional operating region for antenna connected to RWD with 4 W RF output power. Simulated $d_{\max} \approx 75$ cm. RWD, read/write device

transform the damped antenna impedance to R_X. The resonance capacitance C_{par} was determined to be $\frac{1}{\omega_{\text{op}}^2 L} = 55.5$ pF whiles C_h and C_s were 483.83 and 60 pF from Equations (12) and (13), respectively. The equivalent lumped element circuit of the antenna connected to a balanced capacitance matching network was simulated and tuned in the NI AWR Design Environment. The optimized damping and matching circuit parameter values were $R_{\text{par}} = 3.76$ kΩ, $C_h = 374$ pF, and $C_s = 62.50$ pF. The optimized antenna assembly resonates at 13.86 MHz and has an input impedance, $Z_{\text{in}} = 50.34 - j0.0077$ Ω at f_{op} achieving a simulated return loss of about 50 dB at its input port when fed with a 50 Ω source. The tuning and enhancement network was fabricated on FR-4 PCB, connected to the loop antenna. The complete antenna fixture is shown in Figure 11(A). It should be noted that in such a circuit, high rated components were used in order to withstand the high voltage that is generated in the resonant circuit. Furthermore, to deal with parasitics and ensure accuracy of circuit, adjustable components were introduced to allow the tuning of circuit after prototyping. The Γ of antenna-matching circuit assembly was measured using the VNA and tuned for optimal matching at f_{op}. The measurement setup is shown

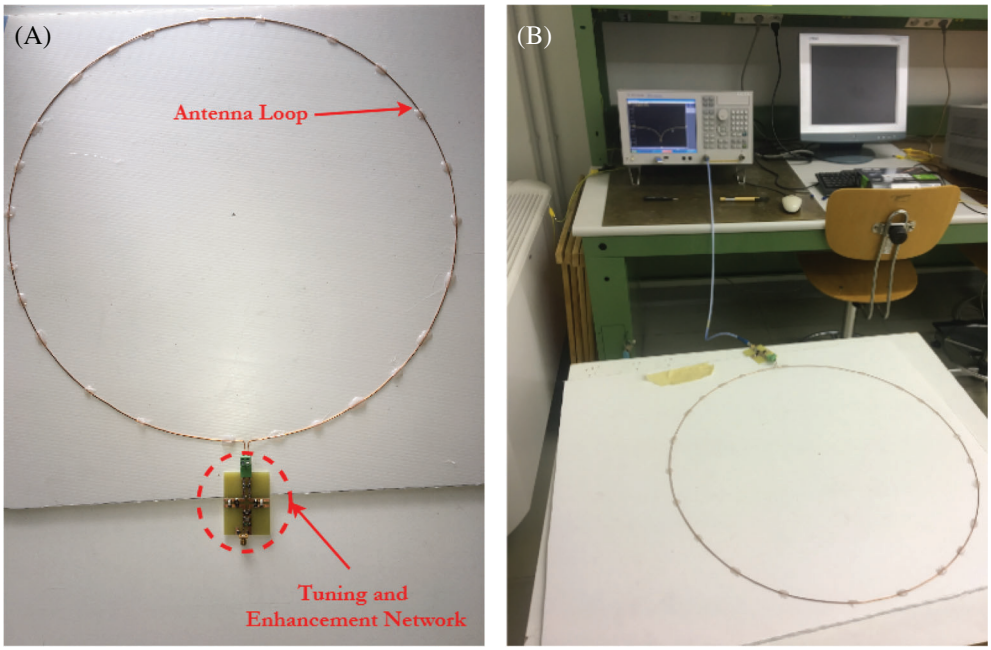

FIGURE 11 Prototype of designed high-frequency antenna and parameter measurement set-up

in Figure 11(B). Plots of the antenna's simulated Z_{in} and Γ as well as that obtained from measurements are shown in Figure 12.

Using the OBID i-scan® ID ISC.2000-A as RWD and NXP ICODE transponders (H_{min}= 0.09 A/m), read range measurements were performed to test the performance of the antenna (Figure 13). The RWD hardware was connected serially (via RS232 interface) to the ID ISOStart measurement software on a computer. The antenna was fed using an RG-58 coax cable. The RF power was set to 4 W and the supply was activated. The current in the loop, I was 0.43 A. The noise floor was first measured to ensure that the amplitude of interference levels was low enough such that tag responses could easily be identified even at low signal levels. A low noise floor was also an indication of a good antenna matching circuit and test environment setup. Recommended noise level values are an average less than 30 mV and a dynamic range of less than 20 mV.[38] The measured noise level had an average value of 6 mV and a dynamic range of about 5 mV. Hence, environmental factors can be assumed to have very little influence on experimental results. The tag was positioned along the RWD antenna perpendicular axis. The distance between the tag and the reader antenna fixture was increased until the magnetic coupling between the two units was severed and card reading was lost. The largest recorded d_{max} was 0.64 m. The simulated d_{max} with the reference tag sensitivity was 0.75 m. An analytical evaluation of the maximum range from system parameters produces a d_{max}= 0.52 m (Equation (15)). The measured and calculated d_{max} are not exactly

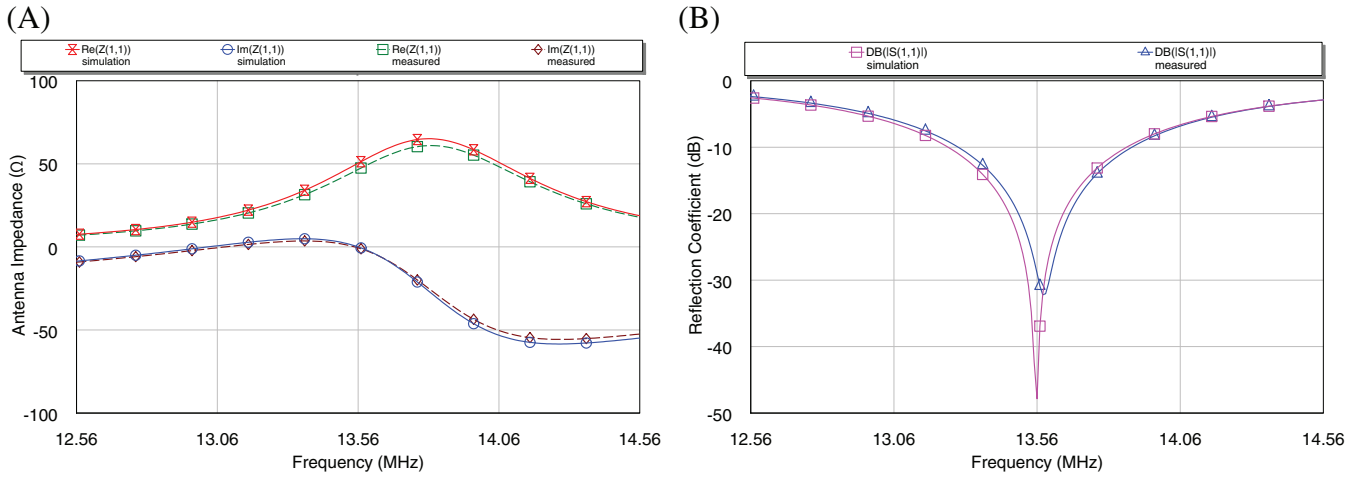

FIGURE 12 Plots of simulated and measured Z_{in}, Γ of complete antenna over a 2 MHz band centered at f_{op}

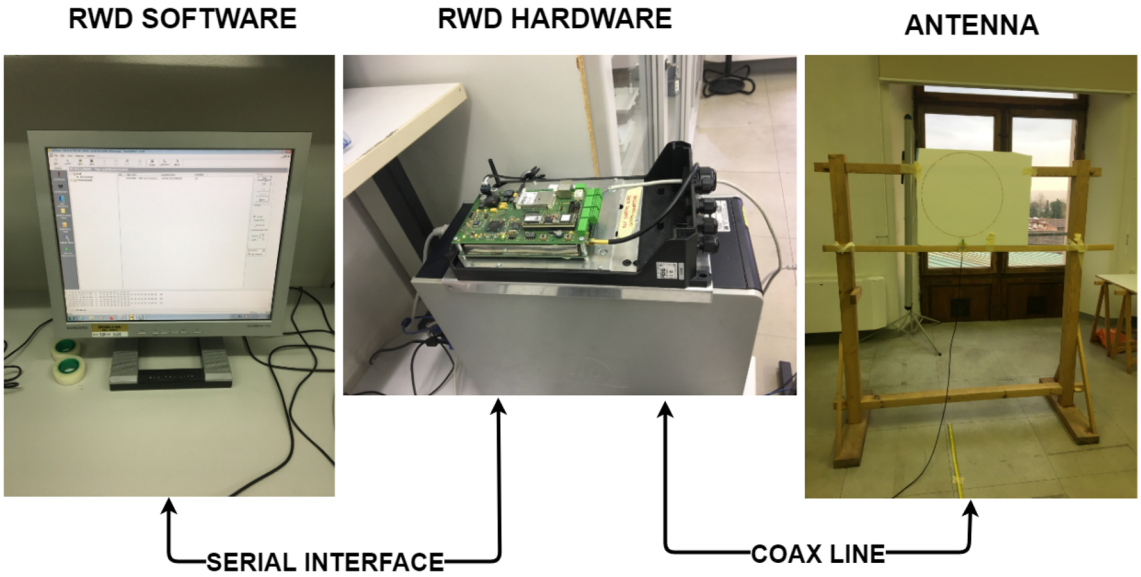

FIGURE 13 Read range test set-up

coincident but bear fair agreement. Thus, the presented model provides a good basis for the antenna design. As indicated in Section 3.1.1, in practical applications, tags would not always be positioned on this axis. A tag positioned at any point in the RWD's interrogation zone will be detected. The point corresponding to $d_{\max}$ represents a limit to the 3D zone. The synthesis of the interrogation zone is treated extensively in References 24,39.

$$d_{\max} = \sqrt{\left(\frac{NIr_d^2}{2H_{\min}}\right)^{\frac{2}{3}} - r_d^2}. \tag{15}$$

5 | CONCLUSION

The presented article describes the development of efficient HF antennas for use in RFID systems operating at 13.56 MHz. Various features and requirements of antennas were discussed and linked to key design parameters such as antenna form-factor and size; RF power level, materials and communication protocol. Tuning circuits necessary to adjust the resonance and power matching characteristics of antennas for good transponder interrogation and response recovery were also discussed. To validate the approaches outlined, a circular loop antenna for a VCD was designed and prototyped. Practical problems associated with the design processes were also commented on. The antenna was fed using an industry standard ISO 15963 compliant RWD and tested for read range performance. The designed antenna with the RWD achieved a good read range which bore fair agreement with the calculated theoretical maximum read range. From these measurement results, it can be concluded that the considerations, methods, and formulas discussed in this article for the design of efficient loop antennas for HF-RFID RWDs, are valid.

PEER REVIEW INFORMATION

Engineering Reports thanks Piotr Jankowski-Mihułowicz and other anonymous reviewers for their contribution to the peer review of this work.

PEER REVIEW

The peer review history for this article is available at https://publons.com/publon/10.1002/eng2.12407.

DATA AVAILABILITY STATEMENT

Data sharing is not applicable to this article as no new data were created or analyzed in this study.

CONFLICT OF INTEREST

The authors declare that there is no conflict of interest regarding the publication of this article.

ORCID

Benjamin Kommey https://orcid.org/0000-0003-3145-0066

REFERENCES

1. Węglarski M, Jankowski-Mihułowicz P, Chamera M, Dziedzic J, Kwaśnicki P. Designing antennas for RFID sensors in monitoring parameters of photovoltaic panels. *Micromachines*. 2020;11:420. https://doi.org/10.3390/mi11040420.
2. Traub K. The GS1 EPCglobal architecture framework, GS1 a.i.s.b.l., v1.6; 2014. https://gs1.org/sites/default/files/docs/epc/architecture_1_6-framework-20140414.pdf. Accessed July 21, 2020.
3. Das R. RFID forecasts, players and opportunities 2019–2029, report, IDTechEx; 2019. https://www.idtechex.com/en/research-report/rfid-forecasts-players-and-opportunities-2019-2029/700. Accessed July 23, 2020.
4. Finkenzeller K. *RFID Handbook: Fundamentals and Applications in Contactless Smart Cards, Radio Frequency Identification and Near Field Communication*. 3rd ed. Hoboken, NJ: Wiley Publishing; 2010.
5. Standard, International Organization for Standardization and International Electrotechnical Commission Cards and security devices for personal identification – contactless vicinity objects – Part 1: physical characteristics. ISO/IEC 15693-1:2018(E). Geneva, CH: International Organization for Standardization; 2018.
6. Standard, International Organization for Standardization and International Electrotechnical Commission Cards and security devices for personal identification – contactless proximity objects – Part 1: physical characteristics. ISO/IEC 14443-1:2018(E). Geneva, CH: International Organization for Standardization; 2018.
7. Standard, International Organization for Standardization and International Electrotechnical Commission Cards and security devices for personal identification – contactless proximity objects – Part 2: radio frequency power and signal interface. ISO/IEC 14443-2:2016(E). Geneva, CH: International Organization for Standardization; 2016.
8. Standard, International Organization for Standardization and International Electrotechnical Commission Cards and security devices for personal identification – contactless proximity objects – Part 3: initialization and anticollision. ISO/IEC 14443-3:2018(E). Geneva, CH: Geneva, CH: International Organization for Standardization; 2018.
9. Standard, International Organization for Standardization and International Electrotechnical CommissionCards and security devices for personal identification – contactless proximity objects – Part 4: transmission Protocol. ISO/IEC 14443-4:2018(E). Geneva, CH: Geneva, CH: International Organization for Standardization; 2018.
10. Standard, International Organization for Standardization and International Electrotechnical Commission Information technology – radio frequency identification for item management – Part 3: parameters for air interface communications at 13.56 MHz. ISO/IEC 18000-3:2010(E). Geneva, CH: International Organization for Standardization; 2010.
11. GS1 EPCglobal EPC Class-1 HF RFID air interface protocol for communications at 13.56 MHz. EPC^{TM} radio-frequency identity protocols, GS1 EPCglobal; 2011.
12. Roz T, Fuentes V. Using low power transponders and tags for RFID applications. EM microelectronic marin n.d:1-8.
13. Standard, International Organization for Standardization and International Electrotechnical Commission Cards and security devices for personal identification – contactless vicinity objects – Part 2: air interface and Initialization. ISO/IEC 15693-2:2019(E). Geneva, CH: International Organization for Standardization; 2019.
14. Aerts W, De Mulder E, Preneel B, Vandenbosch GAE, Verbauwhede I. Dependence of RFID reader antenna design on read out distance. *IEEE Trans Antennas Propag*. 2008;56(12):3829-3837.
15. Balanis CA. *Antenna Theory: Analysis and Design*. Hoboken, NJ: Wiley-Interscience; 2005.
16. Lee Y. *Antenna Circuit Design for RFID Applications*. Vol AN70. Microchip Technology Inc; 2003:1-50.
17. Choudhury MH. In: Mason JW, ed. *Electromagnetism*. Chichester; London, UK: Ellis Horwood; 1989.
18. Yates DC, Holmes AS, Burdett AJ. Optimal transmission frequency for ultralow-power short-range radio links. *IEEE Trans Circuits Syst I Reg Papers*. 2004;51(7):1405-1413.
19. Grandi G, Kazimierczuk M, Massarini A, Reggiani U. Stray capacitance of single-layer solenoid air-core inductors. *IEEE Trans Ind Appl*. 1999;35:1162-1168. https://doi.org/10.1109/28.793378.
20. Texas instruments HF antenna cookbook. Technical application report ; 11-08-28-001; 2001:1-20.
21. Standard, European Telecommunications Standards Institute Short Range Devices (SRD) – Radio equipment in the frequency range 9 kHz to 25 MHz and inductive loop systems in the frequency range 9 kHz to 30 MHz. ETSI EN 300 330 V2.1.0. France, FR: European Telecommunications Standards Institute; 2017.
22. Goulbourne A. HF antenna design notes: technical application report. Technical Report SCBA034. Texas Instruments; 2015.
23. Sittithai P, Phaebua K, Lertwiriyaprapa T, Akkaraekthalin P. Magnetic field shaping technique for HF-RFID and NFC systems. *Radioengineering*. 2019;27:121-sss. https://doi.org/10.13164/re.2019.0121.
24. Li X, Sidén J, Andersson H, Schön T. A paper-based screen printed HF RFID reader antenna system. *IEEE J Radio Freq Identif*. 2018;2(3):118-126. https://doi.org/10.1109/JRFID.2018.2869494.
25. Kirschenbaum I, Wool A. How to build a low-cost, extended-range RFID skimmer. Paper presented at: Proceedings of 15th USENIX Security Symposium, Vancouver, BC, Canada; 2006:43-57.

26. Jacobi R, LaCost E. Antenna design guide for the TRF79xxA: application report. Technical Report SLOA241C; Texas Instruments; 2020.
27. Mirzaee M, Noghanian S, Wiest L, Chang I. Developing flexible 3D printed antenna using conductive ABS materials; 2015:1308-1309
28. Blayo A, Pineaux B. Printing processes and their potential for RFID printing. Paper presented at: Proceedings of the Joint sOc-EUSAI Conference, Grenoble, France; 2005. https://doi.org/10.1145/1107548.1107559
29. Xiao G, Zhang Z, Fukutani H, Tao Y, Lang S. Improving the Q -factor of printed HF RFID loop antennas on flexible substrates by condensing the microstructures of conductors. *IEEE J Radio Freq Identif*. 2018;2(2):111-116.
30. Liu C, Lu D, Yan F, Mei Y. Study of RFID tag antenna manufacturing based on printing technology. *Appl Mech Mater*. 2013;329:135-138. https://doi.org/10.4028/www.scientific.net/AMM.329.135.
31. Lim N, Kim J, Lee S, Kim N, Cho G. Screen printed resonant tags for electronic article surveillance tags. *IEEE Trans Adv Packaging*. 2009;32:72-76. https://doi.org/10.1109/TADVP.2008.2006656.
32. Quintero AV, Molina-Lopez F, Smits ECP, et al. Smart RFID label with a printed multisensor platform for environmental monitoring. *Flexible Print Electron*. 2016;1(2):025003. https://doi.org/10.1088/2058-8585/1/2/025003.
33. Xiao G, Aflaki P, Lang S, et al. Printed UHF RFID reader antennas for potential retail applications. *IEEE J Radio Freq Identif*. 2018;2(1):31-37.
34. Ailian C, Xianming Q, Zhi NC, Boon KL. Performance assessment of printed RFID reader antenna. Paper presented at: Proceedings of the 2007 IEEE Antennas and Propagation Society International Symposium, Honolulu, Hawaii; 2007:301-304.
35. Salmeron JF, Capitan-Vallvey LF, Palma AJ, Molina-Lopez F, Briand D, de Rooij NF. Physical and electrical properties of ink-jet and screen printed patterns for RFID HF antennas. Paper presented at: Proceedings of the IEEE International Conference on RFID-Technologies and Applications (RFID-TA) 2012:188-192. https://doi.org/10.1109/RFID-TA.2012.6404508
36. Petrariu A, Lavric A, Coca E. Design of an high frequency RFID multi-loop antenna for applications in metallic environments. *Adv Electr Comput Eng*. 2018;18:35-40.
37. Thompson T, Locating RF. Interference at HF: a proven and practical approach to dealing with RFI from grow lights and more. *QST*. 2014;33-39.
38. FEIG Electronics GmbH. ID ISC.ANT310310-A HF-antenna datasheet; 2019. https://fccid.io/PJMLRM2000-2/User-Manual/Installation-Manual-1292029.pdf. Accessed October 10, 2020.
39. Jankowski-Mihułowicz P, Węglarski M. Definition, characteristics and determining parameters of antennas in terms of synthesizing the interrogation zone in RFID systems. Radio frequency identification; 2017:65-119; InTech.

How to cite this article: Ofosu Addo E, Kommey B, Selasi Agbemenu A, Kumbong H. On the design and implementation of efficient antennas for high frequency-radio frequency identification read/write devices. *Engineering Reports*. 2021;e12407. https://doi.org/10.1002/eng2.12407